Available online at www.sciencedirect.com
SCIENCE DIRECT®
Journal of the European Ceramic Society 25 (2005) 3553–3561
www.elsevier.com/locate/jeurceramsoc

Processing and characterisation of three-layer alumina-based composites with enhanced damage tolerance

Gürsoy Arslan[a,*], Rolf Janssen[b], Nils Claussen[b]

[a] *Department of Materials Science and Engineering, Anadolu University, Iki Eylul Campus, 26555 Eskisehir, Turkey*
[b] *Advanced Ceramics Group, Technische Universität Hamburg-Harburg, 21073 Hamburg, Germany*

Received 30 April 2004; received in revised form 13 September 2004; accepted 24 September 2004
Available online 19 December 2004

Abstract

Three-layer alumina-based composites reinforced with iron in the inner layer and with chromium in the outer layers were fabricated by first uniaxially pressing the three-layer assembly, followed by cold isostatic pressing at 300 MPa and sintering in a graphite vacuum furnace at 1500 °C for 1 h.

The residual compressive stresses in the outer Cr–Al/Al_2O_3 layers and the residual tensile stresses in the Fe–Al/Al_2O_3 inner layer were predicted as a function of composition and the thickness ratio of the outer and inner layers. Theoretical calculations showed that the compressive stresses in the outer layers increased while the tensile stresses in the inner layer decreased with decreasing outer layer thickness. The existence of compressive stresses was verified by microscopic evidence, which showed that propagation of cracks perpendicular to the interface is suppressed in the outer layer, but promoted in the inner layer.

Indentation and subsequent strength testing showed that these layered composites exhibited improved damage tolerance. Three-layer composites showed four-point bend strengths exceeding the bend strength of unindented monolithic Al_2O_3 even after indentation at 300 N.

Keywords: Milling; Al_2O_3; Laminates; Mechanical properties; Wear parts

1. Introduction

Al_2O_3, the most commonly used wear-resistant technical ceramic, wears most often by grain pluck-out and pop-out caused mainly by the anisotropy of properties such as thermal expansion in different crystal directions. This leads to cracking along grain boundaries that, in turn, will result in two potential wear problems. The first is the hole left on the surface, which allows a high angle of attack for the next abrading particle. Thus, once the initial grain pluck-outs begin, the wear rate can increase. The second problem is that the particle being removed can become an abrading particle itself.[1,2]

In wear applications, hardness is often considered as the critical property, that is, the harder the material, the lower the wear rate. This is, of course, in part true. However, hardness is measured by the resistance of one material to the penetration of another material. Unfortunately, in some applications, the wear is not just a function of indentation depth of a specifically prepared surface; rather, it is wear by the literal removal of material that has been subjected to corrosion, adhesion, material transfer, thermal shock, and Hertzian loads. Properties such as strength, fracture toughness, thermal expansion, thermal conductivity, modulus of elasticity therefore must also be considered in wear applications.[1]

Because most ceramics have lower thermal conductivity than metals, localized heat build up in rubbing or sliding applications must be considered. Too much heat build up from friction can lead to localized thermal stress and thermal shock microcracking, resulting in poorer than expected wear.[1]

Because of the possibility of creating microcracking and reducing wear resistance, localized as well as bulk fracture

* Corresponding author.
E-mail address: garslan@anadolu.edu.tr (G. Arslan).

0955-2219/$ – see front matter © 2004 Elsevier Ltd. All rights reserved.
doi:10.1016/j.jeurceramsoc.2004.09.016

toughness should also be considered. Some examples show that the ability of a ceramic with higher fracture toughness to withstand microcracking from localized loads, thermal shock and thermal stress can offset lower hardness. Toughened ZrO_2 compositions outwear harder Al_2O_3 in some applications, and ZrO_2-toughened Al_2O_3 can significantly outwear normal Al_2O_3 compositions.[1]

Increasing attention has been paid to the design and fabrication of layered composites for tribological applications. In particular, three-layered composites with a symmetric structure have been widely investigated.[3–7] In general, these three-layer laminates are designed to consist of two compressive outer layers and a tensile inner layer.[4–7] It is well known that the mechanical properties of ceramic components for structural applications can be enhanced by the introduction of surface compressive stresses in the outer layers during fabrication.[4,5,8] It is likely that the wear resistance of these composites will also be improved compared to those of single-layer materials. Residual compressive stresses can be generated either by a thermal expansion mismatch between the inner and outer layers or by a volume expansion of a dispersed phase in the outer layers due to phase transformations.[8,9]

The main objective of the present work was to show that the s-3A technology[10,11] (powder mixtures consisting of Al, Al_2O_3 and a metal oxide or a metal are attrition milled, uniaxially pressed, cold isostatically pressed and pressureless sintered under an inert atmosphere in the temperature range of 1400–1550 °C) can be used to fabricate three-layer alumina-based composites with high surface compressive stresses by creating a thermal expansion mismatch between the inner and outer layers. Another objective was to show that the s-3A technology can also be used to tailor physical/mechanical properties important in tribological applications according to the needs.

The three-layer Cr–Al/Al_2O_3//Fe–Al/Al_2O_3//Cr–Al/Al_2O_3 system (3L-Cr-A/Fe-A) was used for the following reasons: (i) Cr/Al_2O_3 and Fe/Al_2O_3 composites can be sintered to high density under basically the same sintering conditions,[12,13] (ii) the interfacial bond strength of Fe and Cr with Al_2O_3 is high[14,15] and (iii) Cr has a lower thermal expansion coefficient than Fe allowing residual compressive stresses to be generated in the outer layers during cooling from sintering temperature.[16]

Table 1
Measured particle size of the starting powders

Powder	d_{10} (μm)	d_{50} (μm)	d_{90} (μm)
A1[a]	9.6	21.3	41.4
Fe[b]	3.2	16.3	43.8
Cr[c]	2.8	13.7	38.0
Al_2O_3[d]		0.2	

[a] Alcan Int., Kingston, Canada.
[b] BASF Carbonyl Iron, Ludwigshafen, Germany.
[c] Alfa Aesar, Johnson Matthey GmbH, Karlsruhe, Germany.
[d] Taimicron TM-Dar, Taimei Chemicals Co. Ltd., Nagano, Japan.

2. Experimental

The d_{10}, d_{50} and d_{90} values of the starting powders as measured with a laser particle size analyser (Mastersizer S, Malvern Ltd., Worchestershire, UK) are shown in Table 1 and the chemical composition of the prepared starting powder mixtures is given in Table 2.

Both Cr–Al/Al_2O_3 (Cr-A) outer-layer and Fe–Al/Al_2O_3 (Fe-A) inner-layer powder mixtures were attrition milled in acetone at 900 rpm for 4–9.5 h depending on the type and amount of metal. 1650 g of 3 mm diameter 3Y-TZP balls were used as the milling medium for a powder charge of 50 g. The attrition milling process was stopped when 90% of the powder particles were finer than about 10 μm with almost no particles being coarser than about 30 μm. After drying in air at room temperature for 48 h, the Cr-A and Fe-A powder mixtures were sieved through a 200 μm screen.

Single-layer Cr-A and Fe-A as well as three-layer 3L-Cr-A/Fe-A specimens were formed by uniaxial pressing (HVP 51 SK, Heinrich Schäfer Maschinenfabrik, Velbert, Germany) at a load of 20 MPa using a 4.5 mm × 47 mm rectangular die. In the case of three-layer specimens, the Cr-A powder mixture was loaded first into the die cavity; then the Fe-A inner-layer powder mixture was added, followed by a second addition of the Cr-A outer-layer powder mixture.

After die pressing, the green specimens were isostatically pressed (KIP 200 ES, Paul Weber Maschinen und Apparatebau, Remshalden, Germany) at 300 MPa for 2 min, and subsequently sintered in a gas pressure-sintering furnace (IBV, Hamburg, Germany) under a vacuum atmosphere. Sintering temperature and sintering time were chosen as 1500 °C and 1 h, respectively while heating and cooling rates were chosen

Table 2
Chemical composition of the prepared powder mixtures

Designation	Al		Fe		Cr		Al_2O_3	
	wt.%	vol.%	wt.%	vol.%	wt.%	vol.%	wt.%	vol.%
15Fe-A	0.9	3.0	13.03	15.0			36.08	82.0
25Fe-A	1.38	5.0	20.11	25.0			28.51	70.0
35Fe-A	2.59	10.0	26.40	35.0			21.01	55.0
15Cr-A	0.31	1.0			12.12	15.0	37.57	84.0
25Cr-A	0.43	1.5			18.88	25.0	30.70	73.5
35Cr-A	0.67	2.5			24.81	35.0	24.52	62.5

as 10 and 30 °C/min, respectively.[12,13,17] Layer thickness was adjusted such that after sintering the total thickness of the three-layer composites was about 6 mm and the ratio of outer layer thickness (t_o) to inner layer thickness (t_i) was either 4 or 8.

Strengths were measured by four-point bending (Universal Testing Machine, Type 1478, Zwick GmbH, Ulm, Germany), using an outer span of 20 mm and an inner span of 10 mm, at a crosshead speed of 0.5 mm/min. The surfaces of the four-point bending specimens (3 mm × 6 mm × 36 mm) were ground and polished down to 6 μm except for the prospective tension side, which was polished down to 1 μm. To evaluate the damage resistance of the 3L-Cr-A/Fe-A composites, polished Fe-A and three-layer specimens were indented at the centre of the prospective tension side using a Vickers diamond pyramid (Type 3212, Zwick, Ulm, Germany) under loads ranging from 10 to 300 N. Care was taken to orient one set of the indentation cracks to be parallel to the longitudinal axis of the rectangular specimens. The indenter contacted the specimen surface for about 25 s before it was withdrawn to complete the load cycle. After indentation, the specimens were immediately tested in four-point bending. Strengths were determined from the average value of five specimens for unindented samples and from that of three specimens for indented samples at each indentation load.

Microstructures were observed by optical (Polyvar 2, Reichert-Jung, Leitz, Wetzlar, Germany) and scanning electron microscopy (FE-SEM, Leo, Type 513, Carl Zeiss, Oberkochen, Germany).

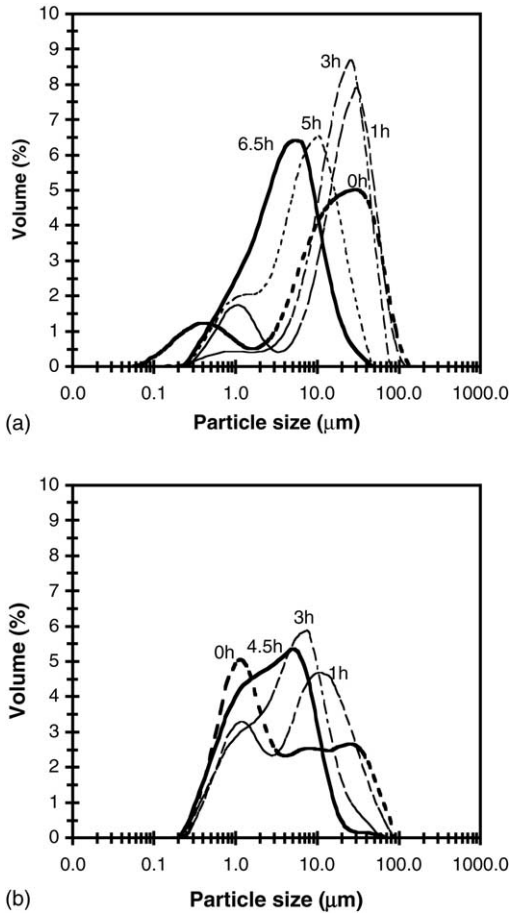

Fig. 1. Particle size distribution of the powder mixtures as a function of milling time: (a) 25Fe-A (25 vol.% Fe, 5 vol.% Al and 70 vol.% Al_2O_3); (b) 25Cr-A (25 vol.% Cr, 1.5 vol.% Al and 73.5 vol.% Al_2O_3).

3. Results and discussion

3.1. Processing

Previous work showed that Fe-A composites with too low or too high Al contents have a relatively high residual porosity content.[12,17] For example, an Fe-A composite containing no Al was shown to have a residual porosity in excess of 8.5 vol.%. The admixed Fe and Al content of the Fe-A composites were therefore adjusted so as to result in composites with residual porosity <5 vol.%. For that purpose, the Al content was adjusted to vary between 3 and 10 vol.%, while the admixed Fe content was less or equal to 35 vol.% (Table 2).

Another work showed that Cr-A composites without any Al contained less than 5 vol.% porosity.[13] Although a systematic study on the densification behaviour of Cr-A composites as a function of the Al content was not undertaken in this work, it was assumed that the densification behaviour of the Cr-A composites is similar to that of the Fe-A composites in that there exists an optimum range of Al content to achieve high density levels (>97% of TD). But, to account for the fact that the residual porosity of Cr-A composites without any Al is less than that of Fe-A composites without any Al, the admixed Al contents in the Cr-A composites were chosen to be less than those in the Fe-A system (Table 2).

The bimodal particle size distribution prior to the milling (Fig. 1) arises from the presence of coarse metal powders and the much finer Al_2O_3 powders that comprise the initial powder mixture (Table 1). Due to the incorporation of coarser ductile Al particles (especially for composites rich in metal content), higher than usual attrition milling speeds and/or increased milling times,[12,13,17] had to be applied to achieve powder mixtures with well mixed fine metal particles.

The change in particle size of two different powder mixtures as a function of milling time is depicted in Fig. 1. After 6.5 h attrition milling, the 25Fe-A powder mixture became monomodal with a d_{90} value of about 11 μm (Fig. 1(a)). For the 25Cr-A powder, a d_{90} value of about 9 μm was achieved after 4.5 h attrition milling (Fig. 1(b)). The attrition milling time for Cr-A powder mixtures was always found to be less than that of Fe-A powder mixtures of similar composition since Fe is more ductile than Cr, and Fe-A compositions contain relatively more of the ductile Al phase (Table 2).

The change in morphology and the gradual comminution of the ductile metal particles with increasing milling time is well depicted in Fig. 2. At higher magnification (Fig. 3),

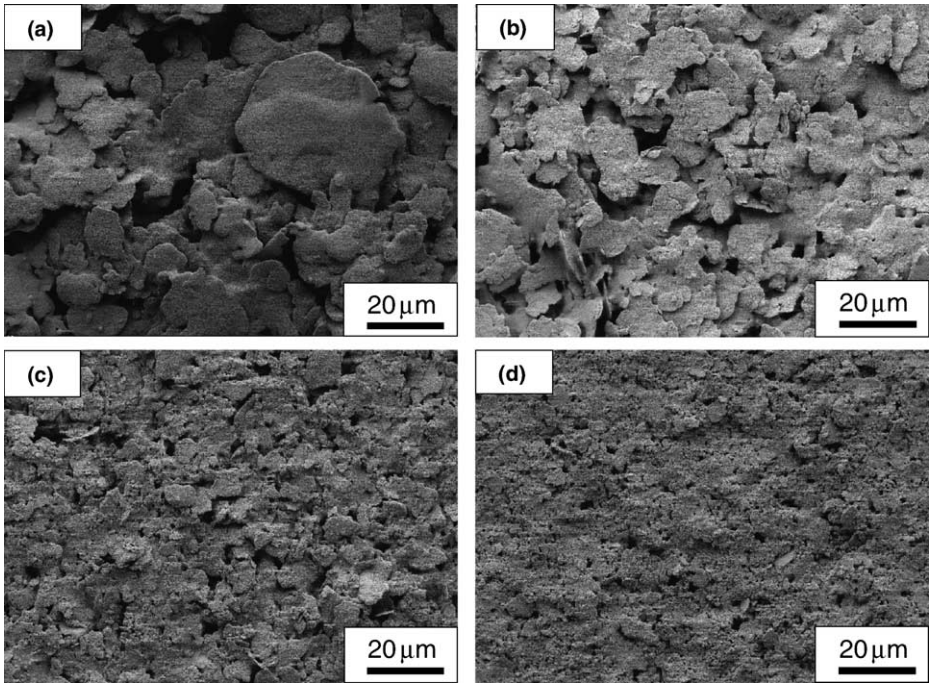

Fig. 2. SEM micrographs showing the change in the particle morphology of the 25Fe-A powder mixture as a function of milling time at 900 rpm: (a) 1 h; (b) 3 h; (c) 5 h; (d) 6.5 h.

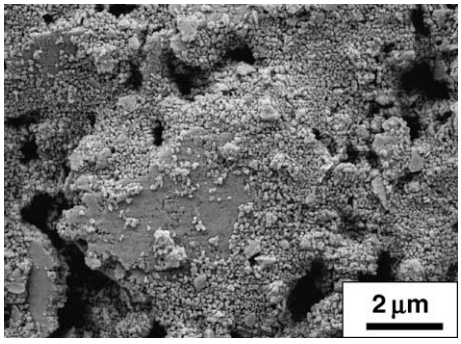

Fig. 3. SEM micrograph of metal particles coated with fine Al_2O_3 powder.

the adhesion of the fine Al_2O_3 particles to the surface of the initially coarse metal powders is clearly seen.

3.2. Characterisation of the interface

Microstructural observations confirmed that the interfacial zone between the outer and inner layers was depleted of metal in all the investigated three-layer composites as is exemplified in Fig. 4. This phenomenon can be explained by considering that Cr and Fe do have some limited solubility for each other.[18] In fact, EDX analyses of the interfacial zone and regions nearby the interface confirmed the mutual diffusion of Fe and Cr in opposite directions over a distance of

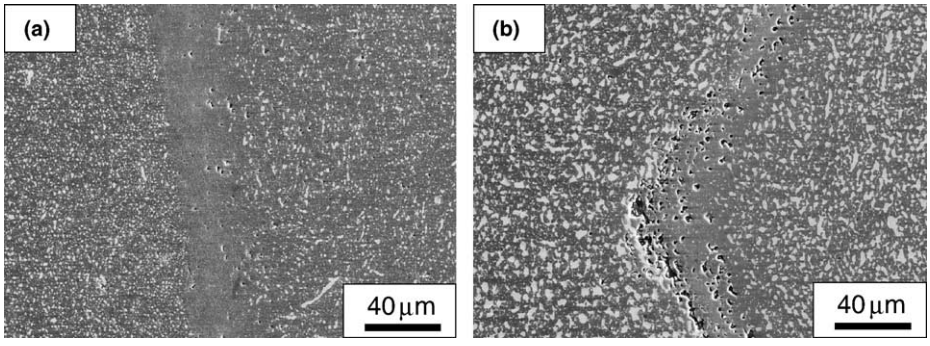

Fig. 4. SEM micrograph showing a transverse section cut of the interface between the outer Cr-A (left to interface) and the inner Fe-A layers (right to interface) in the produced three-layer composites (outer layer thickness ≈1 mm): (a) 3L-15Cr-A/15Fe-A composite; (b) 3L-35Cr-A/35Fe-A composite (with a residual tensile strength exceeding the assumed tolerable tensile strength of 190 MPa in the inner layer).

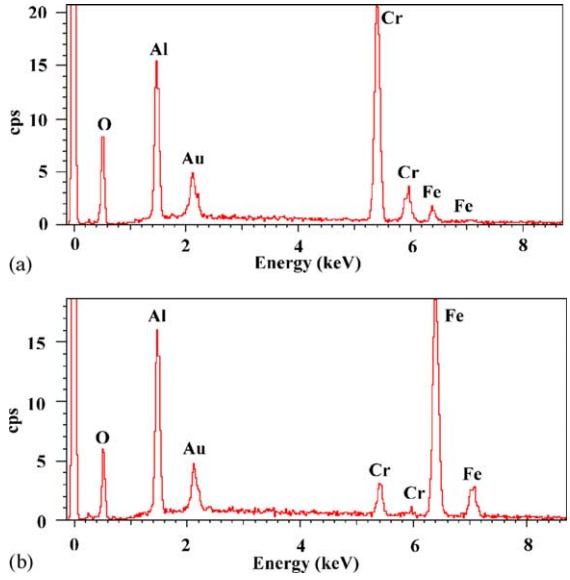

Fig. 5. EDX analysis of a region in the near vicinity of the Cr-A/Fe-A interface: (a) outer layer; (b) inner layer. The Au peak comes from the conductive coating layer which was applied to the SEM specimens to avoid charging.

approximately 10–20 μm with respect to the interface. The EDX analysis of a region in the outer Cr/Al_2O_3 layer close to the interface region is shown in Fig. 5(a). The presence of Fe peaks implies that Fe atoms initially present in the interface zone diffused towards the outer Cr/Al_2O_3 layer during sintering thereby depleting it with respect to Fe. Similarly, Cr atoms may have diffused from the interface zone towards the inner layer (Fig. 5(b)).

It is further seen that pores/microcracks are present at the interface and that the amount of them depends on the chemical composition of the composites. The amount of porosity in composites rich in metal content (Fig. 4(b)) is seen to be significantly higher than those containing less metal (Fig. 4(a)). It is suggested that the chemical composition of the composites affects pore/microcrack formation at the interface via two mechanisms: (i) formation of Kirkendall pores[19] and (ii) creation of a thermal expansion mismatch between the layers.

3.2.1. Formation of Kirkendall pores

It is known that the formation of Kirkendall pores is favoured if the constituent with the lower melting point has a relatively higher solubility in the higher melting point constituent.[19] In fact, the solubility of Al in Fe is ~11 wt.% while the solubility of Fe in Al is low.[18]

Furthermore, since the melting point of Al is significantly less than that of Fe, the diffusivity of Al in Fe is significantly higher than the diffusivity of Fe in Al.[20,21] On the other hand, Al is not expected to diffuse from the interface to the outer Cr-A layer since the solubility of Al in Cr and the solubility of Cr in Al decreases with decreasing temperature. At room temperature, Cr and Al have almost no solubility for each other.[18] Therefore, Al is expected to diffuse preferably from the interface to the inner Fe-A layer while the diffusion of Fe in the backward direction will be limited. As a result, pores will be formed at those points in the microstructure which were previously occupied by Al particles.[19]

The tendency to form Kirkendall pores also increases with increasing Al/Fe ratio of the composition.[22] Consequently, since the Al/Fe ratio (in wt.%) of the composites 3L-15Cr-A/15Fe-A and 3L-35Cr-A/35Fe-A is 0.07 and 0.10 (Table 2), respectively, the tendency to form Kirkendall pores would be promoted additionally in the latter composite.

Another point that may increase Kirkendall pore formation in the composite 3L-35Cr-A/35Fe-A is the fact that the amount of Al oxidised during attrition milling is expected to decrease (and hence the Al/Fe ratio to increase) with increasing metal contents.[17]

3.2.2. Thermal expansion mismatch

The other factor that may contribute to the formation of microcracks at the interface is the thermal expansion mismatch between the layers, which depends on the metal contents in the layers and hence the composition of the starting powders. As will be discussed in Section 3.3, the less the metal contents in the inner and outer layers, the less will be the thermal expansion mismatch, the residual tensile strength in the inner layer and the risk of delamination or microcracking.

3.3. Prediction of residual stresses

During cooling down from the sintering temperature, the inner Fe-A layer would contract more than the outer Cr-A layers if the layers were separated. However, in the case of a well-bonded interface between the layers, the contraction of the inner layer is constrained by the outer layers. This leads to a residual tensile stress in the inner layer, and a residual compressive stress in the outer layers.

Based on the equilibrium of forces in the longitudinal direction, the residual stresses σ_i and σ_o are related by Eq. (1):[4]

$$\sigma_i = -2 \times \frac{t_o}{t_i} \times \sigma_o \quad (1)$$

where σ_i and σ_0 are the residual tensile and compressive stresses in the inner and outer layers, respectively, and t_i and t_o are the thickness of the inner and outer layers, respectively.

The magnitude of the residual compressive stress, σ_o, can be calculated from Eq. (2):[5]

$$\sigma_o = (\alpha_o - \alpha_i) \times \Delta T \times \left(\frac{E_o}{1-\nu_o}\right) \times \left[1 + 2 \times \left(\frac{t_o}{t_i}\right) \times \left(\frac{E_o/(1-\nu_o)}{E_i/(1-\nu_i)}\right)\right]^{-1} \quad (2)$$

where ΔT is the effective temperature difference during cooling, that is, the temperature range in which relaxation processes can be neglected in the residual stress calculations. For simplicity, it was assumed that the composite behaves elastically below its freezing temperature which is set here

Table 3
Material constants of the phases present in the Cr-A/Fe-A system[16,24–27]

Phase	α ($\times 10^{-6}\,^{\circ}C^{-1}$)	ν	E (GPa)
Al_2O_3	8.1	0.22	390
Al	22	0.34	70
Cr	6.2	0.21	279
Fe	12.2	0.39	211

to 1000 °C. E_o, ν_o, E_i and ν_i are the Young's modulus and Poisson's ratio of the outer and inner layers, respectively.

The rule of mixtures was used to estimate the Poisson ratio and thermal expansion coefficients of the layers, while for the calculation of the elastic moduli the Ravichandran equation[23] was made use of.

The material constants needed for the calculation of both the thermal expansion mismatch between the inner and outer layers and the resulting residual stresses are given in Table 3.[16,24–27] The calculated thermal expansion mismatch between the inner and outer layers of the chosen 3L-Cr-A/Fe-A composites is shown in Table 4. The thermal expansion mismatch ($\Delta\alpha$) between the inner and outer layers of the first three 3L-Cr-A/Fe-A composites increases with an equivalent increase in the metal content of the layers. $\Delta\alpha$ is calculated to increase from 0.90×10^{-6} to $2.1 \times 10^{-6}\,^{\circ}C^{-1}$ on increasing the metal content in the layers from 15 to 35 vol.%. Furthermore, comparison of the $\Delta\alpha$ values of the last two compositions indicates that to increase $\Delta\alpha$ between the layers, increasing the Fe content in the inner layer is more effective than increasing the Cr content in the outer layer.

Experimental work has shown that the removal of the layered assembly from the pressing die without spallation at the interfaces between the layers is extremely difficult for the compositions 35Cr-A/35Fe-A and 15Cr-A/35Fe-A. This may be attributed to the significantly different spring back behaviour of the inner and outer layers. Hence, further experimental work was mainly focused on the other three compositions given in Table 4.

The predicted values of the residual tensile and compressive stresses in the three-layer composites are depicted in Fig. 6 as a function of the outer layer thickness (ΔT was assumed as 1000 °C).

Fig. 6(a) and (b) indicate that for a given composition and composite thickness the tensile stresses generated in the inner Fe-A layer increase and the compressive stresses generated in the outer Cr-A layers decrease with increasing outer layer thickness. Hence, to generate high compressive stresses in the outer layers but low tensile stresses in the inner layer, the outer layer thickness should be reduced as much as possible. Nevertheless, since crack initiating flaws are typically in the range of 50–200 μm,[28] the outer layer thickness should be at least 200 μm so as to confine the crack initiating flaws in the compressive zone. However, for the compositions considered in this work, the production of uniform and reproducible layers thinner than 600 μm was found to be unachievable with the simple die-pressing technique employed.

Table 4
Calculated thermal expansion mismatch between the inner and outer layers of the chosen 3L-Cr-A/Fe-A composites

Composition (vol.%)	$\Delta\alpha$ ($\times 10^{-6}\,^{\circ}C^{-1}$)
3L-15Cr-A/15Fe-A	0.90
3L-25Cr-A/25Fe-A	1.50
3L-35Cr-A/35Fe-A	2.10
3L-15Cr-A/35Fe-A	1.72
3L-35Cr-A/15Fe-A	1.28

The calculations also demonstrate that for a given reduction of the outer layer thickness, both the decrease in tensile stress in the Fe-A layer as well as the increase in compressive stresses in the Cr-A layers becomes more pronounced with an increasing mismatch between the thermal expansion coefficients of the Fe-A and Cr-A layers (that is, with increasing metal contents in the inner and outer layers). This trend can also be read off from Fig. 6 since the lines showing the tensile stresses in the Fe-A layer converge while those showing the compressive stresses in the Cr-A layers diverge with decreasing outer layer thickness.

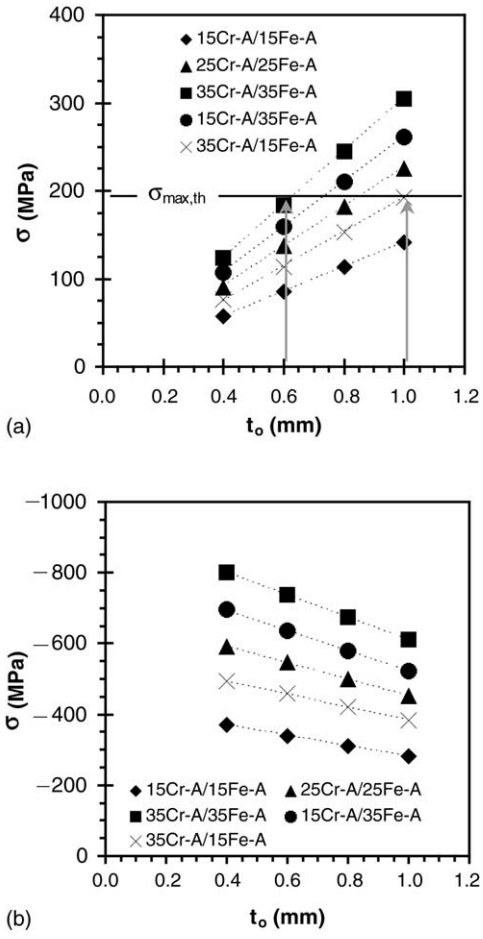

Fig. 6. Predicted residual stresses in the 6 mm thick composites as a function of the outer layer thickness based on Eqs. (1) and (2): (a) tensile stresses in the inner Fe-A layer; (b) compressive stresses in the outer Cr-A layer. Horizontal dashed line in (a) indicates the maximum tolerable tensile stress in the inner Fe-A layer of the three-layer composites obtained from theoretical considerations.

Table 5
Experimentally determined tensile strength (σ_{TS}) values of some transition metal/Al_2O_3 interfaces[15]

Metal	σ_{TS} (MPa)
Cr ($3d^5$)	–
Fe ($3d^6$)	188
Ni ($3d^8$)	116
Cu ($3d^{10}$)	73
Ag ($4d^{10}$)	57

It has been shown by Johnson and Pepper[14] that the strength of the metal/Al_2O_3 interface is a function of the degree of occupation of antibonding orbitals established by the metal–oxygen interaction. The cluster model and molecular-orbital theory predicts a decrease of the metal/Al_2O_3 interface strength in the series Fe, Ni, Cu and Ag. These results correlate very well with the experimentally measured tensile strengths of the respective metal/Al_2O_3 interfaces given in Table 5.[15] Although data for Cr is not given, the Cr/Al_2O_3 interfacial strength should be expected to be even better than that of Fe/Al_2O_3 since Cr possesses less occupied antibonding orbitals than Fe, indicating a stronger adhesion to Al_2O_3.

Based on these considerations and neglecting stress relaxation processes during cooling from high temperatures, the maximum tolerable tensile stress in the inner Fe-A layers was assumed as ~190 MPa (Table 5) in the design of three-layer composites (Fig. 6(a)). Considering three-layer composites with an outer layer thickness of 0.6 mm, delamination and interfacial cracking is not foreseen for the selected compositions (Fig. 6(a)). On the other hand, when the outer layer thickness is increased to 1 mm while keeping the total thickness at 6 mm, the composites 3L-35Cr-A/35Fe-A, 3L-15Cr-A/35Fe-A and 3L-25Cr-A/25Fe-A would be expected to be prone to interfacial cracking while the composites 3L-Cr15-A/Fe15-A and 3L-35Cr-A/15Fe-A are not expected to suffer from this phenomenon (Fig. 4(a)). In fact, pores/cracks were not observed in 3L-15Cr-A/15Fe-A composites (Fig. 4(a)) but in 3L-35Cr-A/35Fe-A composites (Fig. 4(b)). The composite 3L-25Cr-A/25Fe-A was also shown to be prone to interfacial cracking since it is predicted to develop residual tensile stresses somewhat higher than the assumed maximum tolerable tensile stress (Fig. 6(a)). Nevertheless, it may be argued that through relaxation processes taking place at high temperatures the residual tensile stresses are reduced below the tolerable tensile stress thus enabling the fabrication of this layered composite without interfacial cracks.

3.4. Microstructural evidence of compressive stresses

The presence of compressive stresses in the outer Cr/Al_2O_3 layers was furthermore confirmed by microscopic evidence. Fig. 7 shows SEM micrographs of indents made in the inner and outer layers at a distance of about 100 μm form the interface. Fig. 7(a) and (c) show the propagation of cracks in the outer and inner layers after indentation with a load of 100 N, respectively. Similarly, Fig. 7(b) and (d) show the propagation of cracks in the outer and inner layers after indentation with a load of 200 N, respectively. An increase

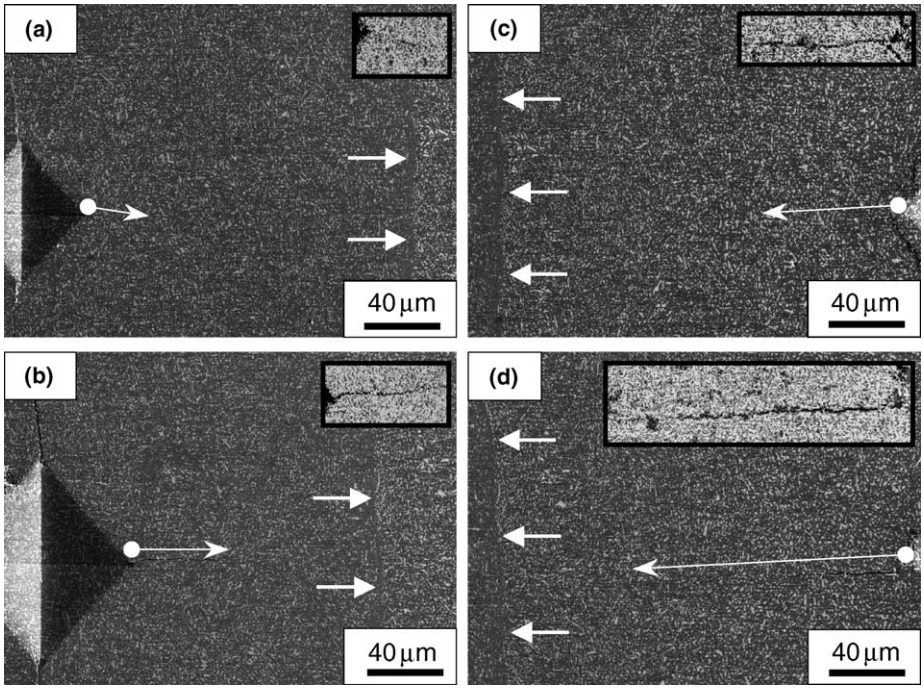

Fig. 7. SEM micrographs of indented 3L-25Cr-A/25Fe-A composites showing the propagation of cracks perpendicular to the Cr-A/Fe-A interface: (a) outer Cr/Al_2O_3 layer after indentation with a load of 100 N; (b) outer Cr/Al_2O_3 layer after indentation with a load of 200 N; (c) inner Fe/Al_2O_3 layer after indentation with a load of 100 N; (d) inner Fe/Al_2O_3 layer after indentation with a load of 200 N. The insets in the upper right corner of the micrographs show an enlarged view of the indentation cracks. The small arrow sets indicate the interface between the outer Cr-A and inner Fe-A layers.

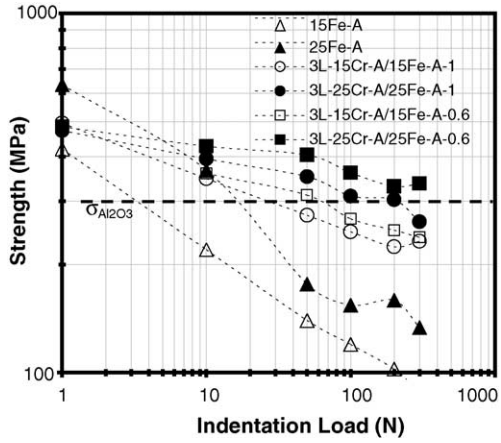

Fig. 8. Variation of the residual bending strength of 6 mm thick Fe-A and 3L-Cr-A/Fe-A composites as a function of indentation load and outer layer thickness. Numbers following the composition labels indicate the thickness of the Cr–Al/Al_2O_3 outer layer in mm. Horizontal dashed line shows the bending stress of unindented monolithic Al_2O_3.

in the indentation load from 100 to 200 N causes an increase in the extension of the cracks in both the outer and inner layers. Nevertheless, it is clearly seen for both indentation loads that the propagation of cracks perpendicular to the interface is strongly suppressed in the outer layers (Fig. 7(a) and (b)), but promoted in the inner layers (Fig. 7(c) and (d)). This indicates that a compressive stress is present in the outer layer, while the inner layer is subject to a tensile stress, as predicted.

3.5. Residual bending strength

The residual bending strength of the indented single-layer Fe-A and 3L-Cr-A/Fe-A composites (6 mm thick) are shown in Fig. 8 for different compositions and outer layer thicknesses.

As is illustrated in this figure, the residual strength of the layered composites is much higher than that of the non-layered reference materials (15Fe-A, 25Fe-A) used here as representatives of non-layered s-3A materials. The strengths of 15Fe-A and 25Fe-A materials deteriorate drastically with increasing indentation load. Single-layered 15Fe-A and 25Fe-A specimens indented at 300 N have a residual strength of only 90 and 135 MPa, respectively. A decrease in residual strength with increasing indentation load is also observed for the layered composites yet the deterioration is far less. 3L-15Cr-A/15Fe-A and 3L-25Cr-A/25Fe-A composites with 1 mm thick outer Cr-A layers indented at 300 N still have a residual strength of 230 and 260 MPa, respectively. A reduction of the Cr-A layer thickness to 0.6 mm brings about a further increase in the composite residual strength. For example, the strength of the 3L-25Cr-A/25Fe-A composite is observed to increase from 260 MPa to 335 MPa, which is even higher than the strength of unindented monolithic Al_2O_3 (which is about 300 MPa). Furthermore, the residual strength of the layered composites seems to have a tendency to remain stable at high indentation loads, at least for composites with an outer layer thickness of 0.6 mm.

It is also seen from Fig. 8 that increasing the metal contents in the inner and outer layers of the starting powder mixture from 15 to 25 vol.% is more effective in improving the residual bending strength of the three-layer composites when compared with reducing the outer layer thickness. For example, an equivalent increase in the metal content of the inner and outer layers of the 0.6 and 1 mm thick three-layer composites from 15 to 25 vol.% brings about an increase in the residual bending strength of about 29 and 32%, respectively. A reduction of the outer layer thickness from 1 to 0.6 mm in the three-layer composites 3L-15Cr-A/15Fe-A and 3L-25Cr-A/25Fe-A, on the other hand, yields an increase in the residual bending strength of about 11 and 14%, respectively. This result is also in agreement with the predicted compressive stresses shown in Fig. 6(b). The compressive stress in the outer Cr-A layer of the three-layer composites is predicted to increase by about 61% on increasing the metal contents in the inner and outer layers from 15 to 25 vol.% (t_o = 1 mm). On the other hand, reducing the outer layer thickness of the composites 3L-15Cr-A/15Fe-A and 3L-25Cr-A/25Fe-A from 1 to 0.6 mm brings about an increase in the compressive strength of only about 21%, in both composites.

3.6. General discussion

The metal reinforced three-layer composites produced via the s-3A technology seem to have somewhat higher unindented bending strength than ceramic–ceramic three-layer composites but are somewhat inferior in terms of retention of the unindented strength values at high indentation loads.[29] The presence of a metal phase in the layers may contribute to the partial relaxation of the residual stresses at high temperatures. Nevertheless, they are expected to be superior in wear applications which apart from hardness require consideration of other physical/mechanical properties. In rubbing or sliding applications where localized heat build up must also be considered, the design of the three-layer composite material would probably depend on the magnitude of the surface compressive stresses desired, the required surface hardness and the thermal conductivity. For example, a three-layer composite with a relatively low Cr content in the outer layer coupled with a relatively high Fe content in the inner layer, such as 3L-15Cr-A/35Fe-A, might be the better choice in wear applications where conduction of heat through the metal rich inner layer is possible. For such applications, a microstructure consisting of a three-dimensionally connected metal network in the inner layer may be most beneficial in achieving high thermal conductivity.[12,17]

On the other hand, the ability of an outer layer with higher fracture toughness to withstand microcracking from localized loads, thermal shock and thermal stress can offset lower surface hardness. For this type of applications, a three-layer composite with relatively higher Cr contents in the outer layers would probably be more suitable. The Fe content in the

inner layer may then be tailored depending on the additional toughness and/or thermal conductivity required and the magnitude of compressive stresses that can be generated in the outer layers.

4. Conclusions

(1) Incorporation of coarse Al powder in the starting compositions necessitated the use of higher milling speeds and/or increased milling times.
(2) In agreement with the theoretical calculations, three-layer composites with reduced surface layer thickness had higher residual strength values for a given composition.
(3) Microstructural investigation of the indented three-layer composites verified the presence of compressive stresses in the surface layers.
(4) Four-point bending tests of indented and unindented three-layer and single-layer composites confirmed the improved damage tolerance of the layered structures.
(5) A relatively higher increase of the residual strength is achieved via adjusting chemical composition when compared with reducing the thickness of the surface layer, in the investigated thickness and composition range.

Acknowledgements

One of the authors (G. Arslan) would like to thank the Turkish Scientific and Technical Research Foundation (TUBITAK) for supporting this work through funding a post-doctoral NATO-B2 scholarship.

References

1. Gauthier, M. M., *Engineered Materials Handbook* (*Desk ed.*). ASM International, USA, 1998.
2. Esposito, L., Moreno, R., Herencia, S. A. J. and Tucci, A., Sliding wear response of an alumina–zirconia system. *J. Eur. Ceram. Soc.*, 1998, **18**, 15.
3. Russo, C. J., Harmer, M. P., Chan, H. M. and Miller, G. A., Design of a laminated ceramic composite for improved strength and toughness. *J. Am. Ceram. Soc.*, 1992, **75**, 3396.
4. Lakshminarayanan, R. and Shetty, D. K., Toughening of layered ceramic composites with residual surface compression. *J. Am. Ceram. Soc.*, 1996, **79**, 79.
5. Sbaizero, O. and Lucchini, E., Influence of residual stresses on the mechanical properties of a layered ceramic composite. *J. Eur. Ceram. Soc.*, 1996, **16**, 813.
6. Wang, H. and Hu, X., Surface properties of ceramic laminates fabricated by die-pressing. *J. Am. Ceram. Soc.*, 1996, **79**, 553.
7. Hillman, C., Sou, Z. and Lange, F. F., Cracking of laminates subjected to biaxial tensile stresses. *J. Am. Ceram. Soc.*, 1996, **79**, 2127.
8. Cutler, R. A., Bright, J. D., Virkar, A. V. and Shetty, D. K., Strength improvement in transformation toughened alumina by selective phase transformation. *J. Am. Ceram. Soc.*, 1987, **70**, 714.
9. Green, D. J., A technique for introducing surface compression into zirconia ceramics. *J. Am. Ceram. Soc.*, 1983, **66**, C-8.
10. Claussen, N., Garcia, D. E. and Janssen, R., German Patent Application DE 4447130, filing date 29 December 1994.
11. Claussen, N., Janssen, R. and Garcia, D. E., Reaction sintering of alumina aluminide alloys (3A). *J. Mater. Res.*, 1996, **11**(11), 2884.
12. Schicker, S., Erny, T., Garcia, D. E., Janssen, R. and Claussen, N., Microstructure and mechanical properties of Al-assisted sintered Fe/Al_2O_3 cermets. *J. Eur. Ceram. Soc.*, 1999, **19**, 2455.
13. Garcia, D. E., Schicker, S., Janssen, R. and Claussen, N., Nb– and $Cr–Al_2O_3$ composites with interpenetrating networks. *J. Eur. Ceram. Soc.*, 1998, **18**, 601.
14. Johnson, K. H. and Pepper, S. V., Molecular-orbital model for metal–sapphire interfacial strength. *J. Appl. Phys.*, 1982, **53**, 6634.
15. Nicholas, M., The strength of metal/alumina interfaces. *J. Mater. Sci.*, 1968, **3**, 571.
16. Ross, R. B., *Metallic Materials Specification Handbook*. Chapman & Hall, London, 1992.
17. Schicker, S., *Herstellung, Characterisierung und Eigenschaften von in situ Fe(Al) und Fe-verstärkten Al_2O_3-Verbundwerkstoffen*. Fortschritt Berichte, VDI Reihe 5 Nr. 526, VDI Verlag, Düseeldorf, 1998.
18. Massalski, T. B. and Okamoto, H., *Binary Alloy Phase Diagrams, Vol 2*. ASM International, 1990.
19. Lee, D. J. and German, R. M., Sintering behavior of iron–aluminum powder mixes. *Int. J. Powder Metall. Powder Technol.*, 1985, **21**(1), 9.
20. Hood, G. M., The diffusion of iron in aluminum. *Philos. Mag.*, 1970, **21**, 305.
21. Raghunathaten, V. S. and Sharma, B. D., Self-diffusion in concentrated Fe–Al and Fe–Si alloys. *Philos. Mag. A*, 1981, **43**(2), 427.
22. Sheasby, J. S., Powder metallurgy of iron–aluminum. *Int. J. Powder Metall. Powder Technol.*, 1979, **15**(4), 301.
23. Ravichandran, K., Elastic properties of two-phase composites. *J. Am. Ceram. Soc.*, 1994, **77**, 1178.
24. Guy, A. G., *Metallkunde für Ingenieure*. Akad. Verl.-Ges., Wiesbaden, Germany, 1983.
25. Vollertsen, F., *Werkstoffeigenschaften und Mikrostruktur*. Hanser, München, 1989.
26. Meyers, M. A., *Mechanical Behavior of Materials*. Prentice-Hall, New Jersey, USA, 1999.
27. Hoper, C. A., *Handbook of Ceramics, Glasses, and Diamonds*. McGraw-Hill, New York, USA, 2001.
28. Virkar, A. V., Huang, J. L. and Cutler, A., Strengthening of oxide ceramics by transformation-induced stresses. *J. Am. Ceram. Soc.*, 1994, **70**, 164.
29. She, J., Scheppokat, S., Scheppokat, S., Janssen, R. and Claussen, N., Reaction-bonded three-layer alumina-based composites with improved damage tolerance. *J. Am. Ceram. Soc.*, 1998, **81**, 1374.